Geochimica et Cosmochimica Acta 390 (2025) 105–116

Contents lists available at ScienceDirect

Geochimica et Cosmochimica Acta

journal homepage: www.elsevier.com/locate/gca

The effect of carbonate chemistry on trace element incorporation in high-Mg calcitic foraminifera

Hagar Hauzer [a,b,*], David Evans [c,d,+], Wolfgang Müller [c,d], Yair Rosenthal [e], Jonathan Erez [a]

[a] The Fredy & Nadine Herrmann Institute of Earth Sciences, The Hebrew University of Jerusalem, Jerusalem, Israel
[b] Israel Oceanographic and Limnological Research, National Institute of Oceanography, Haifa, Israel
[c] Institute of Geosciences, Goethe University Frankfurt, Frankfurt am Main, Germany
[d] Frankfurt Isotope and Element Research Center (FIERCE), Goethe University Frankfurt, Frankfurt am Main, Germany
[e] Department of Marine and Coastal Sciences and Department of Earth and Planetary Sciences, Rutgers University, NB, USA

ARTICLE INFO

Associate editor: Thomas M. Marchitto

Keywords:
Trace elements
Proxies
Carbonate chemistry
Foraminifera
Biomineralization

ABSTRACT

The sodium-to-calcium ratio (Na/Ca) of biogenic $CaCO_3$ has recently been introduced as a proxy for past seawater Ca^{2+} concentrations ($[Ca^{2+}_{sw}]$) as demonstrated by a positive correlation between seawater and shell Na/Ca with a minor influence of salinity. In the present study, we investigate the effect of carbonate chemistry on the Na/Ca proxy by conducting a set of experiments in which pH and the concentration of dissolved inorganic carbon (DIC) were independently varied. In addition to Na^+, the incorporation of Li^+, Mg^{2+}, and Sr^{2+} into the shells of the large benthic high-Mg calcitic foraminifer *Operculina ammonoides* was assessed by culturing under constant DIC (~2170 μmol kg^{-1}) with varying pH (7.5–8.4 NBS scale), and under varying DIC (830–2470 μmol kg^{-1}) with constant pH (~7.9). Foraminiferal growth rate correlates linearly with calcite saturation state (Ω) of the experimental seawater (SW). The lowest pH and DIC experiments were characterized by low population growth rates, and some of these specimens died and their shells partially dissolved.

Na/Ca_{shell} and Li/Ca_{shell} in *O. ammonoides* are positively correlated with SW $[CO_3^{2-}]$ and Ω, whereas Sr/Ca_{shell} and Mg/Ca_{shell} are much less sensitive to these parameters. The relative sensitivity of Na/Ca_{shell} to Ω in *O. ammonoides* is ~ 4 % per Ω unit. However, given that past changes in surface water Ω were probably small relative to changes in $[Ca^{2+}_{sw}]$ the correction for this secondary effect over the Cenozoic is likely to be small. Therefore, we conclude that the sensitivity of *O. ammonoides* Na/Ca to the carbonate system is unlikely to compromise the use of this proxy to reconstruct past $[Ca^{2+}_{sw}]$. In the case of the low-Mg planktic and benthic foraminifera, a data compilation exercise indicates that no resolvable carbonate chemistry effect exists on Na/Ca. Thus, the Na/Ca proxy in benthic nummulitid and planktic foraminifera can be utilized for past $[Ca^{2+}_{sw}]$ reconstructions. Furthermore, coupling this information with the distribution coefficients of other elemental and isotopic systems (e.g., Li^+, Sr^{2+}, Mg^{2+}, K^+, B, $\delta^{11}B$) may allow the reconstruction of wider aspects of past ocean chemistry. Finally, comparison of trace and minor element incorporation into low and high-Mg foraminiferal species, coccolithophores, inorganic calcite, and amorphous $CaCO_3$ (ACC), we propose a modified biomineralization model for hyaline foraminifera centered on SW vacuolization. Foraminiferal data can be explained by a biomineralization process in which high-Mg species utilize a precursor phase (ACC) to produce high-Mg calcite whereas low-Mg species actively remove Mg^{2+} from the site of calcification.

1. Introduction

Past ocean chemistry and climate have covaried through geologic time (e.g., Zeebe and Tyrrell, 2019; Berner et al., 1983). To understand atmosphere–ocean feedbacks, past environmental parameters (mainly temperature, ocean chemistry, and pCO_2) need to be reconstructed. Foraminiferal fossils are abundant and well preserved in oceanic sediments and sedimentary rocks, thus providing unparalleled archives that are ideal for palaeoceanographic reconstructions (e.g., Zachos et al., 2001; Westerhold et al., 2020; Rae et al., 2021). Many trace elements

* Corresponding author at: The Fredy & Nadine Herrmann Institute of Earth Sciences, The Hebrew University of Jerusalem, Jerusalem, Israel.
E-mail address: Hagar.Hauzer@mail.huji.ac.il (H. Hauzer).
+ Now at: School of Ocean and Earth Science, University of Southampton, Southampton, UK.

https://doi.org/10.1016/j.gca.2024.11.022
Received 14 February 2024; Accepted 21 November 2024
Available online 26 November 2024

proxies in foraminiferal shells (El/Ca_{shell}) are measured in relation to Ca and therefore it is important to reconstruct past changes in the seawater (SW) concentration of Ca ($[Ca^{2+}_{sw}]$), which varied through the Phanerozoic (e.g., Horita et al., 2002 and references therein). Recently, the ratio of Na to Ca in foraminiferal shells (Na/Ca_{shell}) has been calibrated and applied as a proxy for past $[Ca^{2+}_{sw}]$ (Hauzer et al., 2018; Le Houedec et al., 2021; Zhou et al., 2021). However, foraminiferal proxies are typically influenced by multiple environmental factors (e.g., temperature and pH in the case of Mg/Ca; Gray & Evans, 2019). In particular, the carbonate chemistry of SW exerts an influence on various elemental and isotopic proxies in foraminiferal shells (Lea et al., 1999; Zeebe and Wolf-Gladrow, 2001; Yu and Elderfield, 2007; Rae et al., 2011; Henehan et al., 2013; Vigier et al., 2015; van Dijk et al., 2017). In the case of the Na/Ca proxy, there are only a few studies which have focused on planktic foraminifera, suggesting a minor effect of SW carbonate chemistry on Na/Ca_{shell} (Lea et al., 1999; Allen et al., 2016). Therefore, to explore the effect of carbonate chemistry on the Na/Ca proxy and other El/Ca_{shell} ratios, we have conducted a carbonate chemistry experiment on the high-Mg large benthic foraminifer *Operculina ammonoides*, a species that has been extensively studied in laboratory cultures (e.g., Evans et al., 2015; Oron et al., 2020; Hauzer et al., 2021). *O. ammonoides* is a nummulitid species that is potentially important for paleo reconstructions as this family of foraminifera are present throughout the Cenozoic (e.g., Brasier and Green 1993; Evans et al., 2018; Martens et al., 2022). In order to further refine palaeoceanographic reconstructions and biomineralization models, we also examined the effect of carbonate chemistry on several other trace element systems (Li^+, Mg^{2+}, and Sr^{2+}).

2. Methods

2.1. Foraminifera collection and culturing

Specimens of *O. ammonoides* were collected from the northern Gulf of Eilat, Israel, at a depth of ~ 22 m in June (HH6) and October (HH7) 2018. Live specimens were identified as those that climbed on vertical glass slides in the laboratory. Live foraminifera were sieved to retain the most abundant size fraction at the time of sampling: HH6: 350–475 μm and HH7: 475–690 μm, following which the specimens were labeled with the fluorescent dye calcein (40 μM) for five days prior to the experiment to visually differentiate between the initial shell and the experimental part grown without the fluorescent dye. For each experiment, one control group of 460 (HH6) or 419 (HH7) specimens was treated with NaOCl, dried, and weighed (average of 205 and 105 μg per individual, respectively) to provide the data necessary to determine growth and to assess the initial weight of the experimental groups. The lower weight per individual of the group composed of larger specimens is due to the evolute growth of the specimens collected for the HH7 experiment. Due to the use of specimens from different size fractions in the two experiment sets, we base any comparative growth rate data on the relative rather than absolute values. Relative growth is calculated as:

$$Growth(\%\ weight\ gain) = 100 \bullet \frac{(CaCO_3\ added)}{initial\ weight}$$

Where $CaCO_3$ added during the experiment was calculated from alkalinity depletion (as in Oron et al., 2020) and the initial weight is the control group weight.

Live foraminifera were divided into 12 experimental groups, containing either 53 (HH6) or 80 (HH7) specimens, grown together in the same jar. All groups were initially incubated in natural Gulf of Eilat SW for 3 days (HH6) and 2 days (HH7), to measure the calcification rates of the populations before exposing them to variable carbonate chemistries. Averaged over all groups, the population growth rates were 6.6±0.17 (HH6) and 2.2±0.19 (HH7) μg $specimen^{-1}$ day^{-1} based on alkalinity depletion. The experimental incubations were conducted in glass jars containing 120 ml of experimental SW that were exposed to 12-hour light–dark cycles of both natural and fluorescent light (~40 μmol photons m^{-2} s^{-1}). During the experiments, salinity, temperature, and illumination were kept constant. The temperature was maintained at 25 ±0.2 °C in water baths with simultaneous cooling and heating. Foraminifera were fed with 50 μl of frozen algae (*Isochrysis*) with each water exchange (every ten days).

2.2. Preparation and characterization of experimental SW

Two experiments were performed: (1) experiment HH6 – variable pH and alkalinity at constant dissolved inorganic carbon (DIC), and (2) experiment HH7 – variable DIC and alkalinity at constant pH (Tables 1, S2-S3). Modified and filtered (GF/F grade) Gulf of Eilat SW was used in both experiments, however, in experiment HH7 the salinity was lowered from ~41 to ~37 on the practical scale with the addition of deionized water (18.2 MΩ cm MilliQ). The effect of salinity on Na/Ca_{shell} in *O. ammonoides* is negligible (Hauzer et al., 2021). Experimental SW reservoirs were spiked with 74 nM ^{135}Ba (Oak Ridge National Laboratory, United States) to unambiguously determine newly grown $CaCO_3$ during the spatially resolved (laser ablation) analysis of the shells (Sec. 2.3; Evans et al., 2015).

To create the variable pH experiment (HH6), either HCl 0.5 mol kg^{-1} or freshly made NaOH 0.5 mol kg^{-1} were gradually added to Gulf of Eilat SW while monitoring the pH until the assigned values were reached (Table 1). Two of the six treatments included elevated $[Ca^{2+}_{sw}]$ (13.7, and 17.7 mmol kg^{-1}, Table 1), achieved by adding $CaCl_2$ (1 mol kg^{-1} stock solution) to the reservoirs. The $[Ca^{2+}_{sw}]$ elevation was designed to decouple the influence of CO_3^{2-}, Ca^{2+}_{sw} and Ω $\left(\Omega = \frac{[Ca^{2+}] \bullet [CO_3^{2-}]}{K^*_{sp}}\right)$. For the variable DIC experiment (HH7), the experimental SW was acidified with HCl 0.5 mol kg^{-1} until pH reached ~ 2.5 to lower the alkalinity close to zero. Next, carbon-free, water-saturated air was bubbled into the acidified SW for 12 h to remove all excess DIC. The salinity remained constant as validated with an optical refractometer RHS-10 (±0.5). To elevate the DIC concentrations to the desired values (Table 1) different amounts of $NaHCO_3$ (0.5 mol kg^{-1}) were added to each reservoir. Finally, the initial pH was adjusted with NaOH and HCl to reach similar initial reservoir pH values for all HH7 treatments (~8.1 ± 0.07 SD).

All experimental reservoirs were kept in collapsible airtight aluminum-coated reservoirs (Supelco 30229-U) to prevent CO_2 exchange with the atmosphere, except for the control treatments (unmodified SW, HH6-3 and HH7-6) that were kept in 1 L pyrex glass bottles wrapped with aluminum foil. During both experiments the dissolved O_2 decreased while DIC gradually increased (Fig. S1) in the collapsible reservoirs, likely due to microbial activity (the alkalinity did not change). This trend was not observed in the control experiments HH6-3 and HH7-6 (kept in glass Pyrex bottles). While the DIC increase in the bags decreased the pH (Fig. S1) the physiology of the foraminifera increased the pH (and the O_2) in the experimental jars, with a net result of returning the chemistry of these seawaters closer to the target values (Fig. S2).

During both experiments, groups of *O. ammonoides* were incubated in glass jars for 10 days between water changes. With every change of the experimental SW, the pH, alkalinity, and dissolved O_2 were measured for both reservoirs and the experimental water (Tables S2-S3). pH measurements were performed with a Radiometer Copenhagen PHM64 Research pH Meter calibrated with NBS buffers. Alkalinity was measured using a Radiometer TIM865 titration manager, with a pHC2401-8 combined pH electrode and SAC950 auto-sampler. Dissolved O_2 was measured with a YSI ProODO optical dissolved oxygen optode, calibrated against Winkler titrations. To estimate the average conditions that the foraminifera experienced during the experiments, the reservoir and experimental jar carbonate chemistry values were averaged (pH and alkalinity) for each treatment (Tables 1 and S2-S3).

Table 1
Experimental SW carbonate chemistry conditions and El/Ca_{sw} for the variable pH (HH6) and variable DIC experiments (HH7). Experiments HH6-3 and HH7-6 were conducted in unmodified SW. Alkalinity and pH were measured while DIC, CO_3^{2-}, and Ω values were calculated using CO2SYS. The values below represent the average of the experimental jars and reservoirs, which we consider to be a good approximation of the average conditions experienced by the foraminifera (except where noted). Separated values of reservoirs and experimental jars are given in Tables S2-S3. The salinity of experiment HH6 was ~41, while HH7 salinity was ~37 on the practical salinity scale. The effect of salinity on Na/Ca_{shell} in *O. ammonoides* is small (Hauzer et al., 2021). Uncertainties are 2SE of all included analyses.

HH6	Res. [Ca_{sw}^{2+}] (mmol kg^{-1})	pH (NBS)	DIC (μmol kg^{-1})	[CO_3^{2-}] (μmol kg^{-1})	Alkalinity (μmol kg^{-1})	Ω	Li/Ca_{sw} (mmol/mol)	Na/Ca_{sw} (mol/mol)	Mg/Ca_{sw} (mol/mol)	Sr/Ca_{sw} (mmol/mol)
1	11.7	7.46 ± 0.12	2109 ± 54	54 ± 18	2125 ± 70	1.3 ± 0.4	2.34 ± 0.006	45.4 ± 3.5	4.83 ± 0.01	8.68 ± 0.04
2	11.7	7.66 ± 0.10	2170 ± 80	87 ± 20	2259 ± 80	2.0 ± 0.4	2.32 ± 0.134	45.5 ± 1.7	4.82 ± 0.26	8.65 ± 0.46
3	11.7	8.06 ± 0.14	2079 ± 40	208 ± 52	2371 ± 94	4.8 ± 1.2	2.40 ± 0.014	47.3 ± 4.6	4.98 ± 0.03	8.89 ± 0.10
4	11.7	8.35 ± 0.11	2195 ± 152	373 ± 74	2722 ± 124	8.5 ± 1.6	2.39 ± 0.016	47.4 ± 5.1	4.97 ± 0.02	8.90 ± 0.05
5 + [Ca_{sw}^{2+}]	13.7	7.80 ± 0.13	2267 ± 118	118 ± 42	2378 ± 106	3.2 ± 1.2	2.04 ± 0.002	40.0 ± 3.1	4.25 ± 0.03	7.63 ± 0.06
6 + [Ca_{sw}^{2+}]	17.7	7.52 ± 0.12	2217 ± 102	64 ± 18	2253 ± 86	2.2 ± 0.6	1.50 ± 0.007	29.4 ± 2.1	3.12 ± 0.04	5.58 ± 0.05
HH7	**Res. [Ca_{sw}^{2+}] (mmol kg^{-1})**	**pH (NBS)**	**DIC (μmol kg^{-1})**	**[CO_3^{2-}] (μmol kg^{-1})**	**Alkalinity (μmol kg^{-1})**	**Ω**	**Li/Ca_{sw} (mmol/mol)**	**Na/Ca_{sw} (mol/mol)**	**Mg/Ca_{sw} (mol/mol)**	**Sr/Ca_{sw} (mmol/mol)**
2	10.65	7.84 ± 0.11	827 ± 40	46 ± 10	919 ± 29	1.1 ± 0.3	2.42 ± 0.002	46.0 ± 0.9	5.03 ± 0.02	8.74 ± 0.03
3	10.65	7.86 ± 0.89	1110 ± 30	63 ± 12	1216 ± 23	1.5 ± 0.3	2.46 ± 0.004	45.3 ± 1.0	5.05 ± 0.02	8.74 ± 0.02
4	10.65	7.82 ± 0.10	1492 ± 60	79 ± 14	1604 ± 41	1.9 ± 0.3	2.45 ± 0.007	46.2 ± 1.0	5.08 ± 0.03	8.75 ± 0.04
5	10.65	7.98 ± 0.08	2050 ± 64	151 ± 24	2254 ± 57	3.6 ± 0.5	2.48 ± 0.004	46.4 ± 2.7	5.10 ± 0.03	8.79 ± 0.06
6	10.65	8.06 ± 0.04	1956 ± 18	172 ± 16	2198 ± 31	4.1 ± 0.4	2.46 ± 0.002	45.8 ± 1.9	5.07 ± 0.01	8.81 ± 0.01
1	10.65	8.00 ± 0.07	2467 ± 44	193 ± 28	2715 ± 59	4.6 ± 0.7	2.49 ± 0.001	46.7 ± 1.2	5.09 ± 0.01	8.79 ± 0.01

We did not include carbonate chemistry values towards the end of an experiment (Fig. 1, marked with crosses) in the calculation of the mean if the specimens did not grow during that period (i.e. measurements from intervals with no net alkalinity depletion). This approach differs slightly to that taken in Coenen et al. (2024), wherein a time-dependent growth rate-weighting was applied to the mean values between the culture and experiment jars. The carbonate chemistry parameters DIC, CO_3^{2-}, HCO_3^-, and Ω were calculated using CO2SYS (Lewis and Wallace, 1998). The values of Ω calculated by CO2SYS use solubility constants for low-Mg calcite. For the relevant solubility product for *O. ammonoides* which has 12 mol% Mg may be higher by a factor of ~ 1.5 compared to the low-Mg calcite. However, due to the wide range of values reported in the literature (e.g., Mucci and Morse, 1983) spanning a factor greater than 10, we base our results and discussion on the values as calculated by CO2SYS. The Ω values of experiment HH6 in which [Ca_{sw}^{2+}] was elevated (HH6-5,6) were corrected to include the [Ca_{sw}^{2+}] addition:

$$\Omega_{corrected} = \Omega \bullet \frac{experiment\ [Ca_{sw}^{2+}]}{natural\ [Ca_{sw}^{2+}]}$$

2.3. Foraminiferal shell chemical analyses

At the end of both experiments (HH6 – 59 days and HH7 – 60 days), all specimens were washed four times with deionized water, dried, and weighed. The specimens were subsequently treated overnight with a dilute (1.5 %) NaOCl solution (Sigma-Aldrich) to remove organic matter, after which the specimens were washed, dried, and weighed again to determine the clean shell mass. The use of NaOCl as an oxidative cleaning agent has been previously shown not to bias foraminiferal Na/Ca ratios measured by LA-ICP-MS depth-profiling (see the supplementary material of Evans et al., 2015) when sufficient rinses with Milli-Q water are performed.

Ten specimens from each treatment with significant growth beyond the calcein mark were selected and analyzed for their trace element/Ca ratios in the Frankfurt Isotope and Elemental Research laboratory (FIERCE) at Goethe University Frankfurt. The analytical method for the determination of trace element concentrations at high spatial-resolution in *O. ammonoides* is described in detail in Evans et al. (2015), and differs here only in that a Thermo Scientific Element XR sector-field inductively coupled plasma mass spectrometer (SF-ICP-MS) rather than a quadrupole instrument was connected to a RESOlution laser ablation system featuring a Laurin Technic S-155 two-volume laser ablation cell.

The ablation of the shell was performed using a laser spot size of 40 μm, a repetition rate of 2 Hz, and fluence of ~ 6 J cm^{-1}. Tuning was performed to achieve maximum sensitivity while maintaining robust plasma conditions, i.e., ThO^+/Th^+ <0.5 %, $Th^+/U^+ = 1 \pm 0.05$, and m/z 22/44 < 2 %. Monitored masses were ^{7}Li, ^{23}Na, ^{24}Mg, ^{25}Mg, ^{43}Ca, ^{88}Sr, and ^{135}Ba, ^{138}Ba. Quantification was achieved following standard practices (e.g., Heinrich et al., 2003) as described in detail in Evans and Müller (2018) and the supplementary materials. Accuracy, assessed by analyzing the USGS calcite standard MACS-3 in an identical way to the samples over the same analytical interval (n = 18) was −11 %, −13 %, 6 %, and −5% for Li/Ca, Na/Ca, Mg/Ca, and Sr/Ca respectively (the key elemental datasets reported here). GOR-128G accuracy relative to NIST

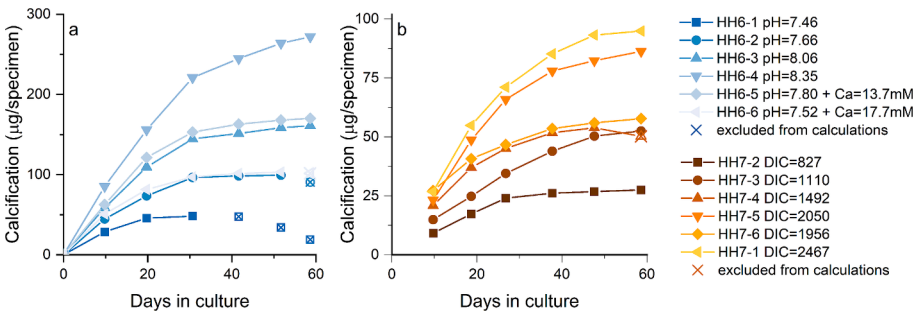

Fig. 1. Calcification curves versus time, based on alkalinity depletion measurements. In some experiments, the specimens stopped growing, these data were removed from growth and carbonate chemistry calculations (marked with crosses). The elevated [Ca_{sw}^{2+}] concentrations in experiment HH6 resulted in a slight increase in growth rate, but the pH effect is much more pronounced. Note that the two experiments were performed on different size fractions of *O. ammonoides*: HH6: 350–475 μm with a mean initial weight of 205 μg specimen^{-1}; HH7: 475–690 μm with a mean initial weight of 105 μg specimen^{-1}.

SRM610 (comparable to the standardization procedure applied to the foraminifera samples; n = 22) was < 1 %. Precision (2SD external repeatability) was 6 %, 9 %, 3 %, and 3 % for the same set of elements respectively, based on repeat analyses of MACS-3 except Mg/Ca (GOR-128G). We note that MACS-3 has a substantially higher [Li] than the foraminifera analyzed here (~950 versus ~ 50 μmol/mol), such that the Li/Ca data quality quoted above may be more favorable than that which is truly applicable to our samples.

Foraminifera shells were analyzed via depth-profiling through the marginal cord along the final 4–6 chambers, with each ablation lasting 50 s (100 laser pulses). Only analyses characterized by the same elevated $^{135}Ba/^{138}Ba$ ratio of the culture SW were considered when calculating mean experiment averages. We note that the lowest pH experiment was characterized by overall very low foraminifera growth rates such that we were only able to perform six analyses on portions of the marginal cord that unambiguously precipitated in culture. While we do report data for this experiment, we note that geochemical characterization of foraminifera should ideally be based on a larger number of analyses in order to average over natural heterogeneity in the population, such that this data point should be treated as preliminary.

3. Results

All results are displayed in Figs. 1-3 and listed in Tables 2-3. In the results and discussion, the apparent distribution coefficient (Hauzer et al., 2018) is calculated as:

$$D_{El} = \frac{(El/Ca)_{shell}}{(El/Ca)_{sw}}$$

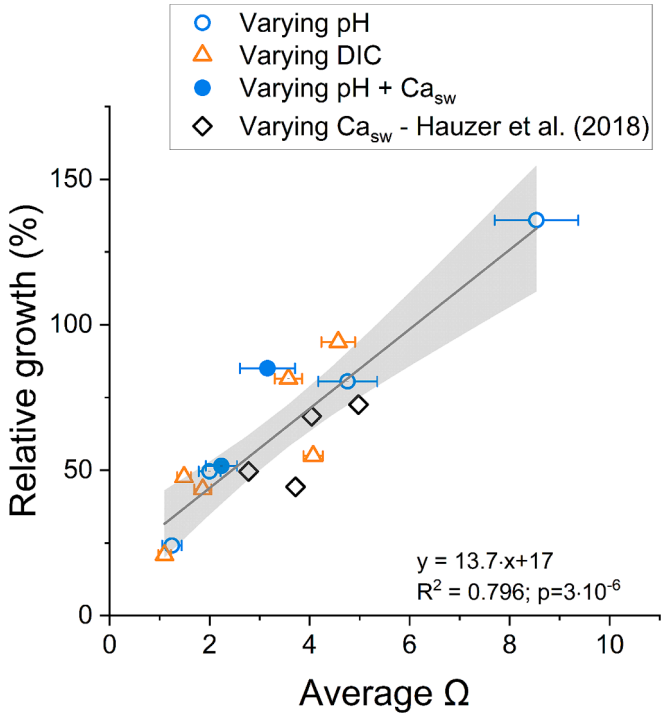

Fig. 2. Average experimental group growth (relative to the control group) versus $\Omega_{calcite}$ including both carbonate system experiments presented here and a previously published *O. ammonoides* variable [Ca^{2+}_{sw}] experiment (Hauzer et al., 2018). The variable [Ca^{2+}_{sw}] experiment of that study was performed with foraminifera from the 475–690 μm size fraction, as in the varying DIC experiment (HH7). In both cases average Ω is the average between the reservoirs and experiments immediately prior to water changes.

3.1. Growth

Shell growth of *O. ammonoides* was measured in two ways: (1) $CaCO_3$ calculated from alkalinity depletion measurements (reservoirs minus incubation jars), referred to here as calcification, and (2) mass gain from final weight measurements compared to the control groups. The variable pH experiment (HH6) contained specimens of the size fraction 350–475 μm. For this experiment, the total growth was 9–136 % (method 1) or 19–145 % (method 2; see Table 2), compared to the control group's initial weight of 205 μg specimen^{-1}. The varying DIC experiment (HH7) was performed with specimens of the size fraction 475–690 μm (initial weight 105 μg specimen^{-1}), and the total growth was (1) 21–94 % or (2) 39–129 % for the two methods, respectively (Table 2). The initial growth rates of the experimental groups in unmodified SW were 6.6 ± 0.17 (HH6) and 2.2 ± 0.19 (HH7) μg specimen^{-1} day^{-1} as measured prior to the carbonate chemistry manipulation. During the first 20–30 days of the experiments the foraminifera maintained growth rates within the range of that observed before the experiment began (Fig. 1), but in the following 30–40 days, the growth slowed down in all groups, and near the end of the experiments some treatments were characterized by bulk dissolution rather than calcification (HH6-1,2,6, and HH7-4; Fig. 1, marked with crosses).

As shown in Fig. 2, both experiments show a positive linear correlation between relative growth and Ω. In two treatments of the HH6 experiment, [Ca^{2+}_{sw}] was elevated (13.7 and 17.7 mmol kg^{-1}, Table 1), which had a negligible amplifying effect on growth compared to modifying SW pH (Figs. 1-2). Further discussion on the growth of the foraminifera can be found in the supplementary information.

3.2. Shell chemistry

Specimens of *O. ammonoides* cultured in the variable DIC experiment (HH7) showed a significant linear increase in all four elements (Na, Li, Mg, Sr) with increasing DIC (Table 3, Fig. 3e-h). However, in the varying pH experiment (HH6), only Na/Ca_{shell}, Li/Ca_{shell}, and Sr/Ca_{shell} increased with increasing pH, whereas Mg/Ca_{shell} showed no resolvable change (Fig. 3a-d). Our Mg/Ca results combined with those of Evans et al. (2018) indicate that with more data we no longer see a significant trend between Mg/Ca and SW pH in *O. ammonoides* (Fig. 3), although a shallow but significant positive relationship remains when relating Mg/Ca to DIC, [CO^{2-}_3], or $\Omega_{calcite}$. The Mg/Ca_{shell} values of Evans et al. (2018) are marginally lower than those reported here, although within 2SD of the present study.

All four elements are plotted against SW carbonate chemistry in Fig. 3, including pH (a-d), DIC (e-h), [CO^{2-}_3] (i-l), and Ω (m-p). El/Ca_{shell} can be fitted as a function of [CO^{2-}_3] or Ω for both experiments, with all elemental ratios characterized by positive correlations with both parameters (Fig. 3 i-p). The only exception to this are the two data points representing experiments in which [Ca^{2+}_{sw}] was increased, in which the Mg/Ca_{shell} and Sr/Ca_{shell} values are much lower (Fig. 3i-p).

4. Discussion

In the discussion we evaluate our experimental results on *O. ammonoides* compared to previous studies on trace element partitioning in foraminifera, coccolithophores, and inorganic calcite experiments as a function of carbonate chemistry.

4.1. The influence of carbonate chemistry on trace element incorporation in O. ammonoides

As shown in Fig. 3 and Table 3, three elements (Na, Li, and Sr) in *O. ammonoides* are affected by SW carbonate chemistry, with El/Ca_{shell} increasing as a function of pH, DIC, [CO^{2-}_3], and Ω. Combining the results of pH and DIC via the common parameters [CO^{2-}_3] or Ω (Fig. 3i-p), it is clear that the latter variables are the dominant factors affecting

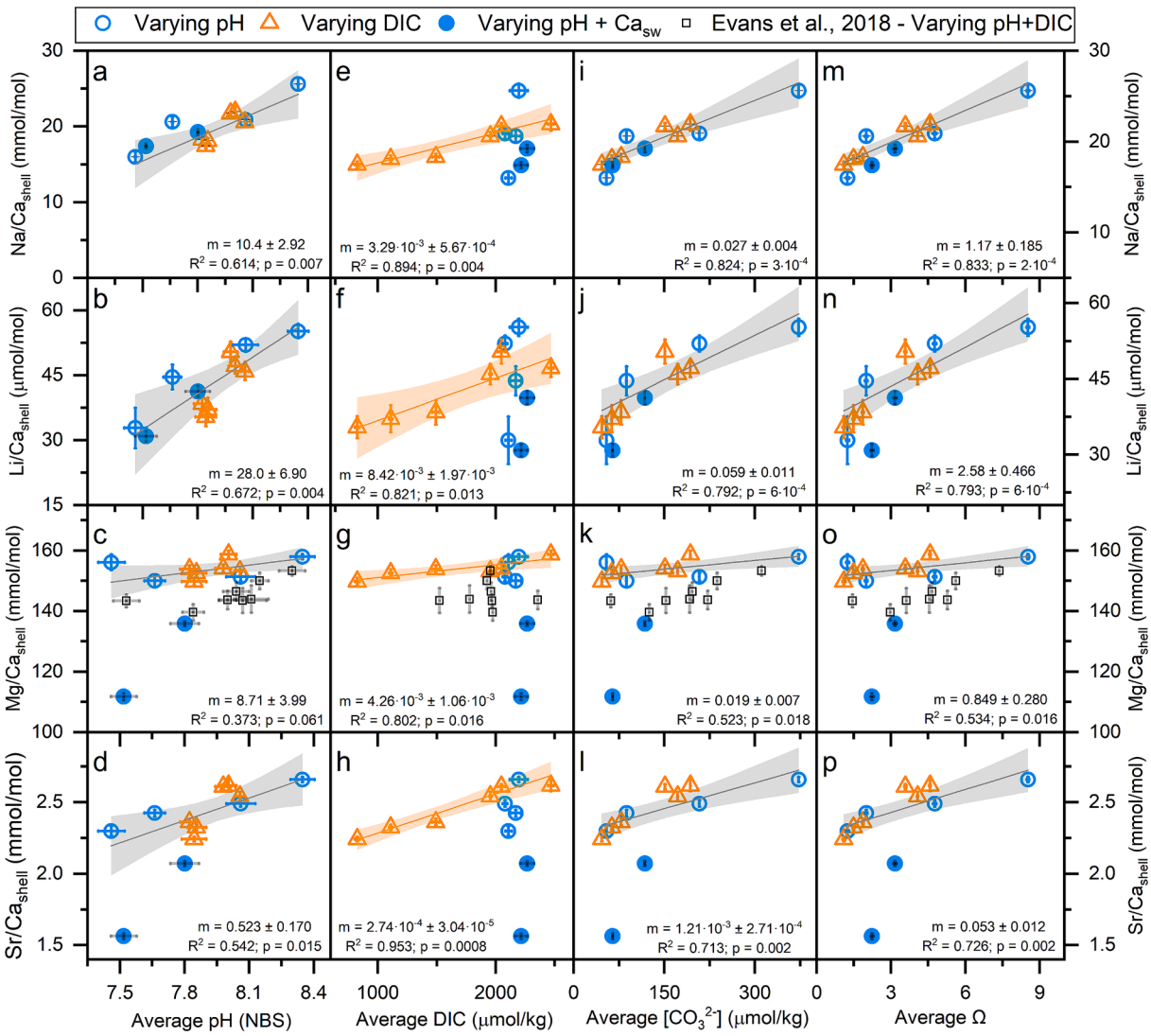

Fig. 3. Cultured *O. ammonoides* shell El/Ca versus SW pH (panels a-d), DIC (e-h), [CO_3^{2-}] (i-l), and Ω (m-p) (Tables 1 and 3). Na, Li, and Sr show positive correlations with pH, whereas no significant relationship exists in the case of Mg/Ca. All elements show a linear increase with increasing DIC, [CO_3^{2-}], and Ω, except for the two elevated [Ca_{sw}^{2+}] points (filled blue circles, Table 1) and therefore these two data points are excluded from the linear fits of all panels. Error bars are 2SE (Tables 1 and 3) and often smaller than the symbols. Full details of the linear regressions are presented in Table S3.

El/Ca_{shell}. The treatments in which [Ca_{sw}^{2+}] (solid blue circles) was changed yield elemental changes that fit very well with the previous variable [Ca_{sw}^{2+}] experiment of Hauzer et al. (2018) (black diamonds in Fig. 4), showing consistency with our previous experimental studies.

Next, we discuss the partitioning (i.e., the apparent distribution coefficients) of the four elements under the hypothesis that hyaline foraminifera calcify by bringing SW vacuoles (SWV) to the biomineralization site (see Sec. 4.3 and e.g., Erez, 2003; Bentov et al., 2009; Evans et al., 2018). The sensitivity of Na/Ca_{shell} and Li/Ca_{shell} to SW carbonate chemistry is higher than for Sr/Ca_{shell} and Mg/Ca_{shell} (Fig. 4; ovals on panels a and b). This divergent response of the alkali elements relative to alkaline-earth elements to SW carbonate chemistry may be related to the single charge of Na^+ and Li^+ and the mechanism of incorporation into the $CaCO_3$ lattice. This was previously discussed by several authors, who suggested that the univalent elements require charge balance either via HCO_3^- substitution for CO_3^{2-} (Land and Hoops, 1973; Füger et al., 2019; Seyedali et al., 2021), or alternatively, that one Na_2CO_3 that replaces two $CaCO_3$ groups, thus causing a CO_3^{2-} vacancy in the lattice (White, 1977, 1978; Busenberg and Plummer, 1985; Yoshimura et al., 2017; summarized in Devriendt et al., 2021). Devriendt et al. (2021) rejected the HCO_3^- hypothesis and strongly support a kinetic argument with higher Na/Ca ratios in the crystal at higher Ω values. In the inorganic experiments of Devriendt et al. (2021), both vaterite and aragonite were precipitated at high Ω, most probably via a precursor amorphous calcium carbonate (ACC), a mechanism which was also proposed for foraminifera (Erez, 2003; Bentov and Erez, 2006; Jacob et al., 2017; Zhu et al., 2021). The relevance of these findings for our observations on *O. ammonoides* is explored in more detail in Sec. 4.3 on biomineralization.

4.2. *Trace element partitioning into inorganic, foraminiferal, and coccolithophore calcite*

A comparison of the data presented here with other hyaline (calcitic radial, perforate) foraminifera that calcify shells with a lamellar architecture (Erez, 2003) is shown in Fig. 5 and S3, mainly including planktic foraminifera as well as a few benthic species in which the SW carbonate system was the main experimental variable (Lea et al., 1999; Russell et al., 2004; Kısakürek et al., 2008; Dissard et al., 2009; Dueñas-Bohórquez et al., 2009; Vigier et al., 2015; Evans et al., 2016; Allen et al., 2016; Holland et al., 2017; Keul et al., 2017; Evans et al., 2018; Roberts et al., 2018; Zhou et al., 2021; Mojtahid et al., 2023). The concentration

Table 2
Total foraminifera growth within each experiment. Calcification was calculated based on alkalinity depletion measurements (reservoirs minus incubation jars) and mass gain from weight measurements. These growth parameters were compared to the initial weight of the control groups, HH6 = 205 μg specimen^{-1} and HH7 = 105 μg specimen^{-1}. Values of calcification do not include the negative Δ alkalinity characteristic of some groups towards the end of the experiment (Fig. 1) or the 2–3 days of initial growth in unmodified SW. The number of growing specimens is based on visible growth beyond the fluorescent calcein marker added immediately prior to the start of the experimental period.

HH6	pH (NBS) ± (2SE)	Total calcification ± 2SE (μg specimen^{-1})	% calcification	Mass gain (μg specimen^{-1})	% mass gain	Growing specimens (%)
1	7.46 ± 0.12	48 ± 26	24	40	19	42
2	7.66 ± 0.10	99 ± 38	50	102	49	83
3	8.06 ± 0.14	161 ± 50	81	170	83	94
4	8.35 ± 0.11	272 ± 64	136	298	145	96
5 + [Ca^{2+}_{sw}]	7.80 ± 0.13	170 ± 54	85	193	94	90
6 + [Ca^{2+}_{sw}]	7.52 ± 0.12	103 ± 40	52	118	58	89
HH7	DIC (μmol kg^{-1}) ± 2SE	Total calcification ± 2SE (μg specimen^{-1})	% calcification	Mass gain (μg specimen^{-1})	% mass gain	Growing specimens (%)
2	827 ± 40	28 ± 8	21	40	39	48
3	1110 ± 30	53 ± 8	48	75	72	74
4	1492 ± 60	54 ± 16	43	56	53	62
5	2050 ± 64	86 ± 18	81	114	109	74
6	1956 ± 18	58 ± 20	55	76	73	57
1	2467 ± 44	95 ± 20	94	134	129	63

Table 3
Shell chemistry of *O. ammonoides* cultured under varying pH, [Ca^{2+}_{sw}], and DIC (Tables 1). Only analyses characterized by elevated $^{135}Ba/^{138}Ba$ (n) were used to calculate the average El/Ca_{shell}. Uncertainties are 2SE of all included analyses.

HH6	n	pH (NBS)	Li/Ca_{shell} (μmol/mol)	Na/Ca_{shell} (mmol/mol)	Mg/Ca_{shell} (mmol/mol)	Sr/Ca_{shell} (mmol/mol)
1	6	7.46 ± 0.12	32.9 ± 9.36	16.0 ± 1.34	156 ± 5.24	2.30 ± 0.064
2	14	7.66 ± 0.10	44.6 ± 5.76	20.6 ± 1.26	150 ± 4.10	2.42 ± 0.050
3	17	8.06 ± 0.14	52.0 ± 3.22	20.9 ± 1.08	151 ± 2.74	2.49 ± 0.044
4	27	8.35 ± 0.11	55.2 ± 3.34	25.6 ± 1.54	158 ± 1.76	2.66 ± 0.036
5 + [Ca^{2+}_{sw}]	24	7.80 ± 0.13	41.3 ± 2.58	19.2 ± 0.82	136 ± 1.56	2.07 ± 0.034
6 + [Ca^{2+}_{sw}]	21	7.52 ± 0.12	30.9 ± 2.44	17.4 ± 0.64	112 ± 2.22	1.56 ± 0.038
HH7	n	DIC (μmol/kg)	Li/Ca_{shell} (μmol/mol)	Na/Ca_{shell} (mmol/mol)	Mg/Ca_{shell} (mmol/mol)	Sr/Ca_{shell} (mmol/mol)
2	26	827 ± 40	35.4 ± 4.40	17.5 ± 0.70	150 ± 2.40	2.24 ± 0.032
3	24	1110 ± 30	37.1 ± 5.36	18.1 ± 0.72	153 ± 2.50	2.32 ± 0.032
4	26	1492 ± 60	38.4 ± 4.80	18.3 ± 0.70	154 ± 2.40	2.36 ± 0.044
5	28	2050 ± 64	50.4 ± 4.78	21.7 ± 0.60	154 ± 2.46	2.61 ± 0.034
6	27	1956 ± 18	46.0 ± 4.06	20.6 ± 0.88	153 ± 2.90	2.54 ± 0.060
1	34	2467 ± 44	47.2 ± 3.54	21.9 ± 1.48	159 ± 2.42	2.62 ± 0.080

of the four elements Na^+, Li^+, Mg^{2+}, and Sr^{2+} is much higher in the high-Mg *O. ammonoides* compared to the low-Mg species. While *O. ammonoides* Na/Ca_{shell} and Li/Ca_{shell} (Fig. 5 and S3) is sensitive to carbonate chemistry (as is also the case for K/Ca; Nambiar et al., 2023), no resolvable effect can be observed in these elements for the planktic species. Li/Ca_{shell} of the intermediate-Mg calcite species *Amphistegina* (3–4 mol% Mg; Vigier et al., 2015; Roberts et al., 2018) is characterized by a moderate positive relationship with Ω (Fig. 5b and S3b). Most planktic species show a decrease in Mg/Ca with increasing pH or $[CO_3^{2-}]/Ω$ (Lea et al., 1999; Russell et al., 2004; Kısakürek et al., 2008; Allen et al., 2016; Evans et al., 2016; Holland et al., 2017), which has been mechanistically related to pH in some studies (Evans et al., 2016; Gray and Evans, 2019), in part because in several experiments that varied DIC no such trend is observed (Dissard et al., 2009; Dueñas-Bohórquez et al., 2009). Evans et al. (2016) suggested that the low pH interferes with the process of Mg removal from the site of calcification, thus resulting in higher Mg/Ca_{shell} (see sec. 4.3). In contrast, the benthic, low-Mg calcite foraminifer *Ammonia* sp. is characterized by a very low Mg concentration and no Mg/Ca-Ω trend (Dissard et al., 2009; Keul et al., 2017). In the case of Sr/Ca, all species show a linear increase with Ω (Fig. 5d, S3d). In the low Mg planktic species *O. universa* (Allen et al. 2016), this trend was observed whether or not foraminifera were cultured under elevated [Ca^{2+}_{sw}] (~18.5 mmol kg^{-1}; Fig. 5d). The significance of these observations regarding changes between D_{El} as a function of Ω when either [Ca^{2+}_{sw}] or [CO_3^{2-}] are changed will be discussed in the next section, in comparison to inorganic calcite precipitation experiments.

As relevant background information we note that intracellular calcification in coccolithophores is centered on ion transport through membranes with precipitation occurring in a large coccolith vesicle (Taylor et al., 2012 and references therein). In other marine eukaryotic calcifiers (e.g., foraminifera, corals, mollusks, sea urchins) precipitation of $CaCO_3$ commences from solutions that are similar (or identical) to SW with partial control by the organism. Endocytosis of SW and elevation of pH (and likely DIC) initiating calcification has been demonstrated for several foraminiferal species (e.g., Erez, 2003; Bentov et al., 2009; de Nooijer et al., 2009; Evans et al., 2018). Where we discuss D_{El} values for inorganic calcite and ACC, we use those from experiments precipitated from solutions similar to SW unless otherwise noted. In these inorganic experiments, precipitation kinetics strongly increases the partition coefficients of many cations with distribution coefficients < 1 (D_{El} of Na, Li, Sr, and Mg; e.g., Lorens, 1981; Mavromatis et al., 2013; Füger et al., 2019; Gabitov et al., 2019; Devriendt et al., 2021). ACC precipitated from SW is characterized by D_{El} values ~ 1–2 order of magnitude higher

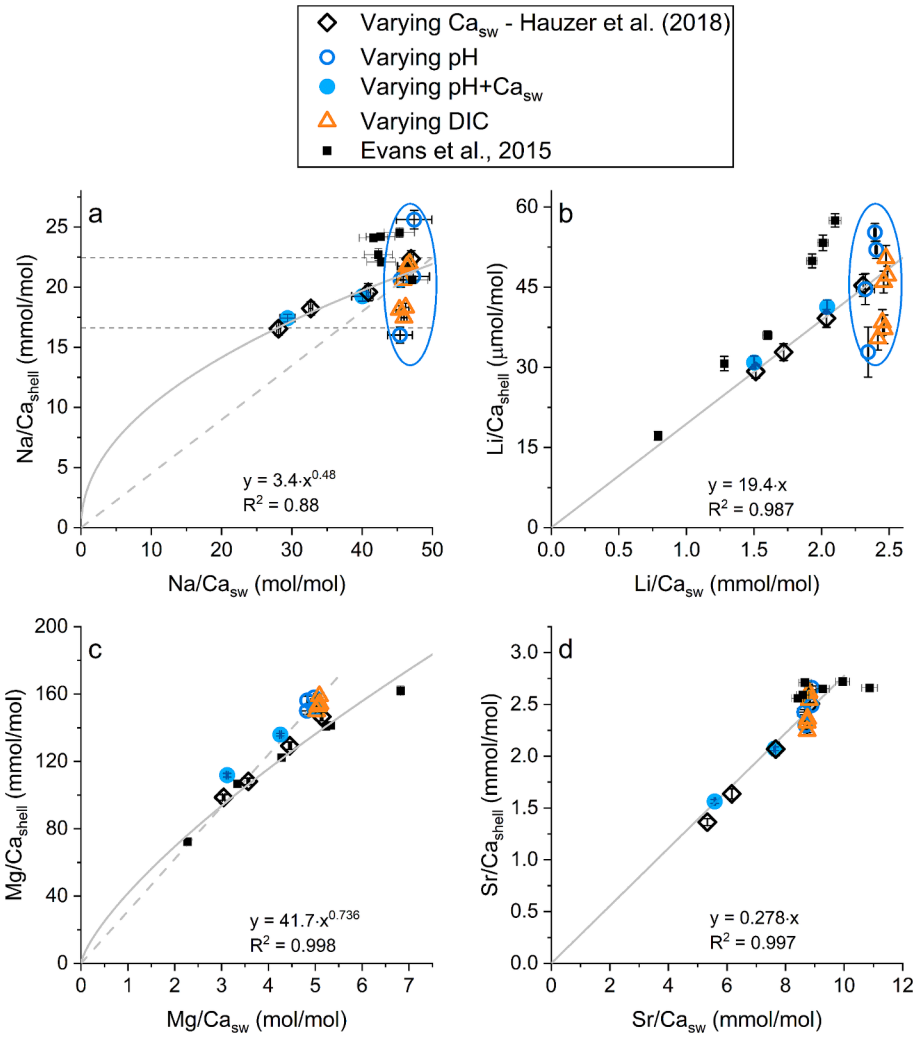

Fig. 4. *O. ammonoides* El/Ca_{shell} versus the respective SW values, combining the results of the [Ca^{2+}_{sw}] experiment (Hauzer et al., 2018) with the carbonate system experiments of this study (Table 1) and of Evans et al. (2018), and the seawater Mg/Ca experiments of Evans et al. (2015). Linear regressions are fitted through the entire dataset. Note that the varying pH + [Ca^{2+}_{sw}] treatments (HH6) agree well with the varying [Ca^{2+}_{sw}] experiment of Hauzer et al. (2018) and for Na and Mg are fitted with a power curve. The carbonate system experiments are characterized by a large degree of variability in Na/Ca and Li/Ca that is not related to [Ca^{2+}_{sw}] (bounded by the ovals in a and b). In contrast, Mg/Ca and Sr/Ca are characterized by a low degree of variability with SW carbonate chemistry compared to the control exerted by [Ca^{2+}_{sw}]. Error bars are often smaller than the symbols.

than inorganic calcite (except D_{Li}) or aragonite and requires very high Ω (e.g., Evans et al., 2019, 2020).

In *O. ammonoides*, the four elements reported here increase with increasing pH and/or DIC, [CO_3^{2-}], and Ω (Fig. 3), which may be explicable via higher calcification rates (Fig. 2). However, foraminiferal calcification rates (e.g., Fig. 2) may be different from inorganic crystal growth rates because calcification is intermittent and often characterized by diurnal cycles. With this caveat in mind, in *O. ammonoides*, D_{El} does not correlate with calcification rates for any of the four elements discussed here (Fig. S5), suggesting that kinetics may not play a major role in explaining differences between foraminiferal species and inorganic calcite. Alternatively, population calcification rates may not be a good proxy for actual crystal growth rate in foraminifera, while the similarity between the Ω-D_{El} slopes in inorganic and high-Mg foraminiferal calcite (Fig. 5) may imply a role for kinetic effects. In view of the differences in kinetics and the mother solution between biogenic and inorganic minerals we discuss the partition of each element separately.

Magnesium: D_{Mg} values in *O. ammonoides* are very high (2.7 ± 0.06•10^{-2}) compared to low Mg foraminifera (~10^{-3}) and coccolithophores (~3•10^{-5}, e.g., Müller et al., 2021), implying a strong degree of biological control on the incorporation of this element. D_{Mg} values in inorganic calcite are similar to those of *O. ammonoides* (1.7•10^{-2} – 2.5•10^{-2}; Mucci and Morse 1983; De Choudens-Sanchez and Gonzalez, 2009), while ACC precipitated from SW-like solutions has a higher D_{Mg} of ~ 9•10^{-2} (Evans et al., 2020). In echinoderms, ACC is a precursor phase to their high-Mg calcite (e.g., Aizenberg et al., 1996; Beniash et al., 1997; Addadi et al., 2003). Given the overall similar calcite Mg/Ca to echinoderms, we therefore suggest a role of ACC in the high-Mg *O. ammonoides*. Foraminifera are characterized by a very large variability in D_{Mg} (e.g., Bentov and Erez 2006; Fig. 6), ranging between D_{Mg} = 2.7•10^{-2} in *O. ammonoides* to ~ 1•10^{-3} in planktic and deep benthic species (Table S5), implying that the various processes mentioned above operate to varying degrees in different species. The fact that inorganic calcite D_{Mg} is ~ 20 times higher than that of the low-Mg foraminifera supports a Mg-removal mechanism in low-Mg species, as suggested by Zeebe and Sanyal (2002; see sec. 4.3).

Strontium: Foraminiferal D_{Sr} ranges between ~ 0.15 in the low-Mg species to 0.28 in the high-Mg *O. ammonoides* (Fig. 6 and Table S5). In ACC, D_{Sr} is high (~0.6–0.8; Evans et al., 2020), and in inorganic calcite the range is 0.15 < D_{Sr} < 0.4 in SW like solutions (Mucci & Morse, 1983) and 0.02 < D_{Sr} < 0.2 in Mg-free solutions (Fig. 5 in Geerken et al., 2022). In foraminifera, Ω (and other carbonate system parameters) exert some

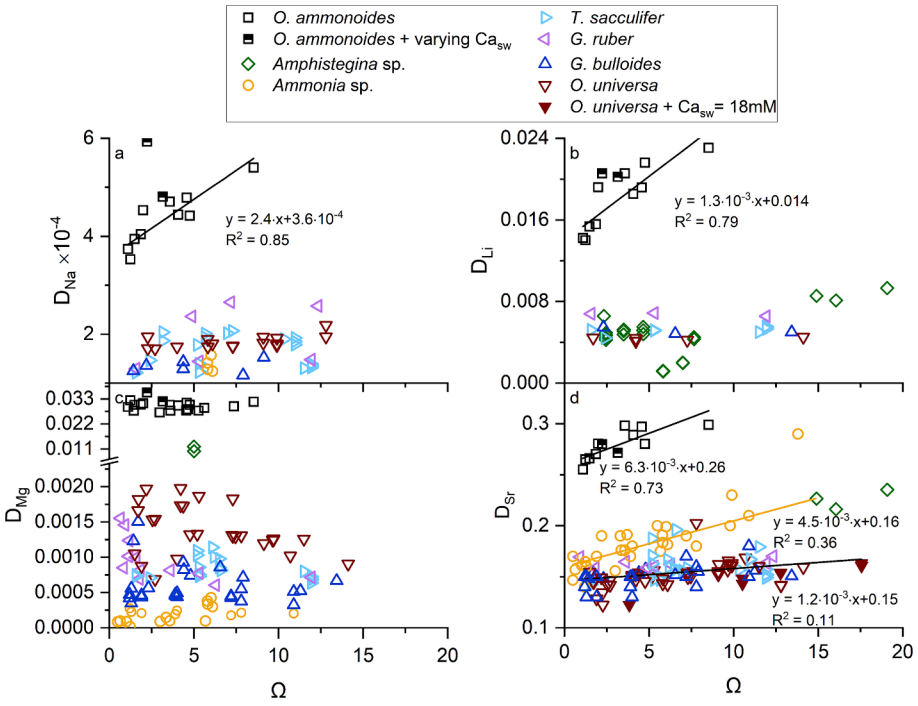

Fig. 5. The apparent distribution coefficients of each element versus Ω based on a compilation of data for all species cultured under variable SW carbonate chemistries. Note that: i) all planktic species fall on one $\Omega_{calcite}$-D_{Sr} trend line despite the difference in Sr/Ca_{sw} (compare panel d with Fig. S3d) in the higher $[Ca^{2+}_{sw}]$ experiment of Allen et al. (2016), and ii) the low-Mg benthic species *A. tepida* is characterized by a steeper $\Omega_{calcite}$-D_{Sr} slope than the other low-Mg species. Only statistically significant trends are plotted in the figure.

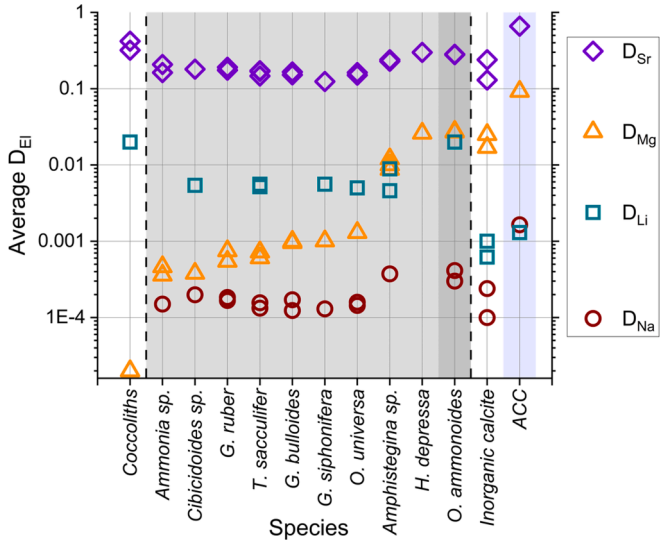

Fig. 6. Average apparent distribution coefficients (D_{El}) of coccolithophores (transmembrane transport dominated), several species of hyaline foraminifera (gray shading), inorganic calcite, and amorphous calcium carbonate (ACC; blue shading). The values plotted here along with a complete list of sources are given in Table S5 and Fig. S4.

control on D_{Sr} (e.g., Yu et al., 2014; Lawson et al., 2024) with different slopes (Fig. 5d), pointing to a deviation from the purely inorganic process of Mg-driven lattice distortions impacting Sr incorporation (e.g., Evans et al., 2015 and references therein). Coccolithophore D_{Sr} (0.46; Müller et al., 2021) is higher than all foraminiferal species (Fig. 6). A positive trend between D_{Sr} ($0.1 < D_{Sr} < 0.65$) and calcification rates in coccolithophores was ascribed to the rate-dependent discrimination of Ca^{2+} versus Sr^{2+} during transport across ion channels/pumps (e.g., Stoll and Schrag 2000; Rickaby et al., 2002).

Sodium: In *O. ammonoides* D_{Na} ($3•10^{-4}$) is slightly higher but similar to that of Kitano et al. (1975) for inorganic calcite (SW-like solutions; $D_{Na} = 2.4•10^{-4}$). Other studies have reported D_{Na} ~ 3 times lower ($D_{Na} = 1•10^{-4}$; Mg-free solutions; Okumura & Kitano 1986; Füger et al., 2019). In high-Mg foraminifera, D_{Na} is correlated with shell Mg/Ca, implying a possible mineralogical control on D_{El} of alkali elements (Evans et al., 2015; van Dijk et al., 2017), although this cannot explain the results from our carbonate chemistry experiment given that this exerted minimal control on shell Mg/Ca. However, in the case of the planktic foraminifera, D_{Na} is similar to inorganic calcite (Füger et al., 2019) again suggesting an overall calcite Mg/Ca effect when considering all species, and providing evidence that their calcifying fluid is Mg depleted. The high D_{Na} and D_{Mg} in *O. ammonoides* may also be related to an ACC precursor given that D_{Na} and D_{Mg} in ACC are much higher than inorganic calcite (Fig. 6). In *O. ammonoides*, Ω has an additional strong influence on Na/Ca and Li/Ca (Fig. 4) possibly due to their involvement in the alkalinity and pH elevation of the calcifying fluid via Na^+/H^+ transporters, discussed below.

Lithium: The inorganic calcite and ACC D_{Li} values derived from experiments conducted in SW-like solutions are similar (D_{Li} = 1-2•10^{-3}; Table S5, Fig. 6 and S4). When other solutions are used, a large range of D_{Li} values are observed (Okumura and Kitano, 1986; Füger et al., 2019; Seyedali et al., 2021; Marriott et al., 2004). In biogenic carbonates (foraminifera and coccolithophores) D_{Li} is much higher than most inorganic precipitates (Fig. 6 and S4, and Table S5), suggesting a strong biological control on this element. The higher biogenic D_{Li} values cannot be accounted for by a possible ACC precursor because D_{Li} of ACC is low (similar to inorganic calcite; Fig. 6). Therefore, we propose that both D_{Na} and D_{Li} are influenced by Na^+/H^+ transporters as shown for coccolithophores (Taylor et al., 2012) and for eukaryotic cells based on δ^7Li (Vigier et al., 2015; Poet et al., 2023). In SW, Li^+ is a micro-element (0.025 mM) while Na^+ is the major cation (470 mM). For this reason, the activity of Na^+/H^+ transporters (pH elevation) is less visible on Na^+ partitioning while the co-transported Li^+ results in a larger increase in

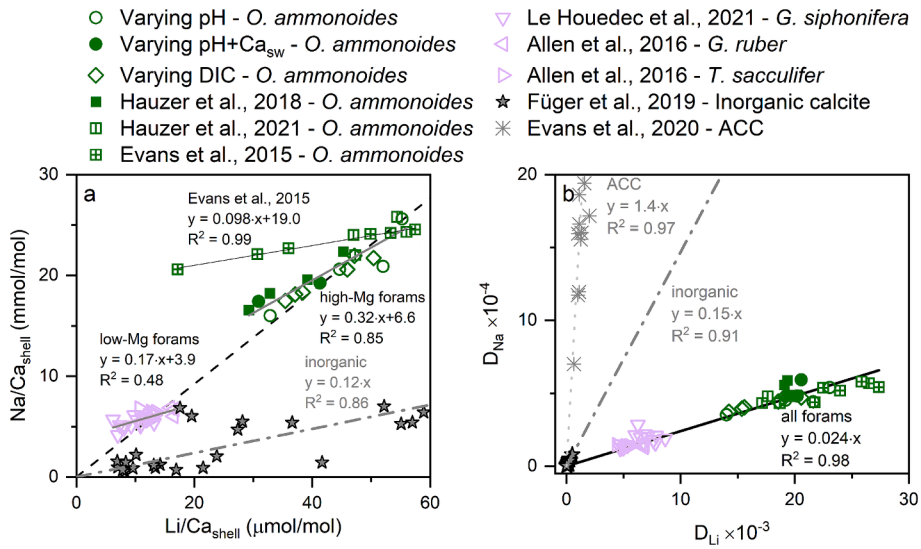

Fig. 7. (a) Na/Ca_{shell} versus Li/Ca_{shell} and (b) D_{Na} versus D_{Li} in all cultured foraminifera from studies reporting data for both elements. The dashed line in panel a is the linear fit through all the foraminiferal data forced through the origin ($y = 0.46 \bullet x$; $R^2 = 0.98$). The shallower slope of Evans et al. (2015) results from the use of artificial SW with a non-natural $[Li^+]$. Similarly, $[Li^+_{sw}]$ in the inorganic experiment plotted here was 10× higher than SW. In panel b, all foraminiferal data can broadly be fitted by a single linear relationship (including that of Evans et al., 2015), demonstrating that this relationship is not markedly different when $[Li^+_{sw}]$ is varied. Foraminiferal D_{Li} is higher than in inorganic calcite by a factor 5–20, possibly due to Li^+ transport (see Sec. 4.3).

D_{Li}. Moreover, Na/Ca_{shell} and Li/Ca_{shell} are tightly correlated (Fig. 7 and S6) for all experiments with *O. ammonoides* (Hauzer et al., 2018, 2021; and this study). More broadly, a linear regression between D_{Na} and D_{Li} is observed for both high and low-Mg foraminiferal species (Fig. 7b). Inorganic calcite and ACC show higher D_{Na} versus D_{Li} slopes compared to foraminifera, which broadly fall on a single relationship across species, possibly due to the much higher D_{Li} in foraminifera (Fig. 7).

4.3. Insights into foraminiferal calcification processes

Two broad mechanisms have been proposed for the transport of ions to the site of calcification in hyaline foraminifera. The SWV model involving SW vacuoles (e.g., Erez, 2003; Bentov et al., 2009; Evans et al., 2018), and the transmembrane Ca^{2+} transport (TMT) model (e.g., Nehrke et al., 2013; de Nooijer et al., 2014). The SWV model (Fig. 8) posits that:

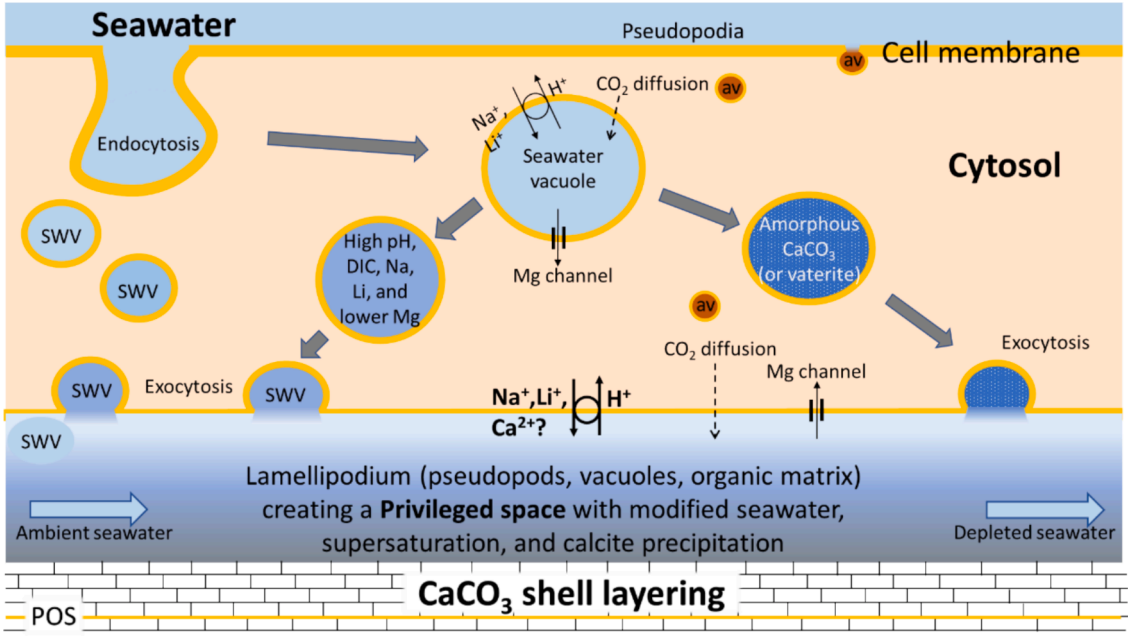

Fig. 8. Generalized calcification model for secondary calcite precipitation in hyaline foraminifera using SW vacuoles (SWV; modified from Bentov et al., 2009; Bentov and Erez, 2006; Erez, 2003). The surrounding SW is engulfed via endocytosis to form SWV in which pH and alkalinity increase is achieved by active proton removal against cations (e.g., Na^+; represented by the darker blue vacuoles). In parallel, CO_2 diffusion into the vacuoles (possibly from acidic vesicles – av) elevates the DIC and CO_3^{2-} while Mg may be transported to the cytosol. Within the calcification site (privileged space), secondary calcite is precipitated over the primary organic sheet (POS, yellow line) in the presence of organic matrix molecules which determines the shape of the new chamber and the crystals orientation. Continuous precipitation of calcitic radial layers occurs under SW transport, with supersaturation maintained by addition of SWV (possibly with ACC) and by further alkalinity increase at the site of shell formation.

1. The observed endocytosis of SWV (e.g., Bentov & Erez, 2005; Bentov et al., 2009) is likely followed by an increase in pH (Bentov et al., 2009; de Nooijer et al., 2009) and DIC to increase Ω. This possibly leads to precipitation of amorphous $CaCO_3$ (ACC; see Arns et al., 2022) and/or vaterite (Jacob et al., 2017) prior to the formation of high-Mg calcite (e.g., *Operculina* sp. ~ 12 mol%, *Heterostegina* sp. ~ 12 mol%, *Pararotalia* type ~ 20 mol%, and *Amphistegina* sp. ~ 3–4 mol% and many others; e.g., Bentov and Erez, 2006). In inorganic experiments utilizing high-Mg solutions (e.g., SW) the transformation from ACC to calcite results in high-Mg calcite (e.g., Blue et al., 2017).
2. In the case of the low and intermediate-Mg species calcification proceeds as described above, possibly with additional transport of Mg out of the SWV and the privileged space thus resulting in lower concentrations (e.g., Zeebe and Sanyal, 2002).

We propose that all foraminifera need to elevate the pH and the DIC in the SWV in order to precipitate $CaCO_3$. pH elevation requires active transport of protons from the SWV to elevate their pH from 8.1 (SW) to ~9 (e.g., Bentov et al., 2009; de Nooijer et al., 2009). We propose that proton-ATPase and Na-ATPase, are involved in this process, as suggested by Taylor et al. (2012) for the coccolithophores. Because Na^+ and Li^+ are both alkali elements and have similar ionic radius, Li^+ may be co-transported via Na^+-ATPase when it is active (e.g., Maloy, 1990). Because Li^+ is a trace element (0.025 mM) its increase in the SWV and eventually in the calcite shell is pronounced. This is supported by the higher Li^+ in foraminiferal shells and also in coccolithophores compared to inorganic calcite (5–20 times; Fig. 6 and Table S5). This mechanism was proposed to explain both the high Li/Ca and more positive Li isotopic composition of *Amphistegina lobifera* in the experiments of Vigier et al. (2015). The applicability of this hypothesis is more broadly supported by the strong correlation between Na/Ca and Li/Ca for the foraminifera in general (Fig. 7) and by the fact that many other calcite precipitating organisms have a higher D_{Li} than inorganic calcite (Ulrich et al., 2021). The large difference in D_{Li} and D_{Na} between high and low-Mg foraminifera may indicate a differential use of proton transporters between these groups, although we also note that a mineralogical control on Na/Ca has been proposed (Evans et al., 2015). The high sensitivity of Na/Ca and Li/Ca to the carbonate system in high-Mg species (Fig. 5) is therefore well explained by the proton transport processes.

The process of Mg-removal from SWV or the site of shell formation in low and intermediate-Mg species (as suggested by Zeebe and Sanyal, 2002; Erez, 2003; Bentov and Erez, 2006; Evans et al., 2018) is supported by the D_{Mg} of planktic foraminifera which is ~ 20 times lower than inorganic calcite (Fig. 6 and Table S5). Therefore, planktic species that utilize SWV need to lower the calcification site Mg to ~3–4 mmol kg^{-1} to produce calcite with the observed D_{Mg} values (Table S5).

4.4. The reliability of Na/Ca as a proxy for $[Ca^{2+}_{sw}]$

Na/Ca_{shell} in the high-Mg *O. ammonoides* is sensitive to Na/Ca_{sw} and also to changes in SW carbonate chemistry (Fig. 5 and S3). Although our data indicate a similar sensitivity of Na/Ca to the carbonate system and $[Ca^{2+}_{sw}]$ (Fig. 4), our experimental $\Delta CO_3^{2-} = \sim 350$ µmol kg^{-1} exceeds the long-term change over the past 100 Ma ($\Delta CO_3^{2-} = \sim 100$ µmol kg^{-1}, Zeebe and Tyrrell, 2019) whereas the experimental $[Ca^{2+}_{sw}]$ (10–18 mmol kg^{-1}) is less than the likely magnitude of change over the same interval (10–30 mmol kg^{-1}). As such, long-term reconstructions are unlikely to be biased by this complication, particularly if Ω is the controlling carbonate system parameter on alkali element incorporation into these foraminifera, given that this has remained within tight bounds since the mid-Mesozoic (e.g., Zeebe & Tyrell, 2019). However, Na/Ca-derived $[Ca^{2+}_{sw}]$ reconstructions across events with rapid ocean carbonate chemistry changes may be biased, if these cannot be corrected for. In some archives, it is possible to reconstruct SW carbonate chemistry using other proxies (e.g., B/Ca, B isotopes, S, or other anion as has recently been demonstrated in the case of foraminifera or corals; van Dijk et al., 2017, Lawson et al., 2024, Ram and Erez 2023, respectively). If such information is available, it may be possible to correct Na/Ca data for SW carbonate chemistry changes in the high-Mg species studied here. Finally, we note that since Sr/Ca and Mg/Ca in *O. ammonoides* are much less sensitive to changes in SW carbonate chemistry (Figs. 3-5), and Na/Ca and Li/Ca are tightly correlated in low and high-Mg foraminifera (Fig. 7), it may be that all four elements can be used within a multi-proxy framework to reconstruct past SW $[Ca^{2+}]$. In the case of low-Mg foraminifera, Na/Ca_{shell} is insensitive to changes in the carbonate system (Fig. 5a and S3a). Therefore, we conclude that when using the species-specific Na/Ca proxy in low-Mg species, reconstructing past $[Ca^{2+}_{sw}]$ apparently does not require a carbonate system correction (Zhou et al., 2021).

5. Summary

In this study we experimentally determined the effects of SW carbonate chemistry (varying pH and varying DIC) on the incorporation of trace elements into the shells of the high-Mg calcite large benthic foraminifer *Operculina ammonoides*. In particular, we tested the validity of the Na/Ca proxy for determining past $[Ca^{2+}_{sw}]$ as suggested for large benthic and planktic foraminifera, and corals (Hauzer et al., 2018; Zhou et al., 2021; Le Houedec et al., 2021; Ram and Erez 2021). We found that the incorporation of Na^+ and Li^+ into *O. ammonoides* is sensitive to changes in SW carbonate chemistry, whereas Mg^{2+} and Sr^{2+} are only weakly affected by carbonate chemistry compared to changes in El/Ca_{sw}. However, given that we cannot distinguish between an $\Omega_{calcite}$ and $[CO_3^{2-}]$ control in our experiments we suggest that the decoupling of Ω and $[Ca^{2+}_{sw}]$ during the last 100 Ma (Zeebe & Tyrell, 2019) means that long-term SW carbonate chemistry changes are unlikely to be a substantial source of uncertainty when applying the Na/Ca proxy. Thus, measurements from *O. ammonoides* can complement data from low-Mg planktic species, for which it has been shown that Na/Ca_{shell} and Li/Ca_{shell} are not sensitive to carbonate chemistry changes (e.g., Allen et al., 2016).

The distribution coefficients of elements in different foraminiferal species compared with inorganic calcite, amorphous calcium carbonate (ACC), and coccolithophores (that possess an endmember biomineralization pathway in which there is a tight cellular control on calcification), indicate that most low-Mg foraminiferal species actively remove Mg^{2+} from the calcifying fluid, while the high-Mg benthic foraminifera studied here do not. Further work is required to understand the implications of a metastable or amorphous precursor phase in the case of both organisms, particularly concerning the geochemistry of the ACC-calcite transformation. A tight correlation between Na/Ca and Li/Ca is observed in both foraminiferal and inorganic calcite that may indicate a kinetic control on both elements. However, all biogenic calcites compiled here have much higher D_{Li} compared to inorganic precipitates, to a first-order approximation indicating that Li^+ enrichment in the calcifying fluid may be a feature of the biomineralization process of a wide range of marine organisms. It is possible that Li^+ is transported into the calcifying fluid during the pH elevation of the SW vacuoles mediated by Na^+/H^+-ATPases or K^+/H^+-ATPases.

Finally, we conclude that foraminifera are ideal organisms for palaeoceanographic reconstructions because they precipitate their shells directly from seawater using endocytosis (seawater vacuoles).

CRediT authorship contribution statement

Hagar Hauzer: Writing – review & editing, Writing – original draft, Visualization, Validation, Software, Project administration, Methodology, Investigation, Formal analysis, Data curation. **David Evans:** Writing – review & editing, Validation, Software, Resources, Project administration, Methodology, Investigation, Formal analysis, Data curation, Conceptualization. **Wolfgang Müller:** Writing – review &

editing, Funding acquisition. **Yair Rosenthal:** Writing – review & editing, Validation, Supervision, Resources, Funding acquisition, Conceptualization. **Jonathan Erez:** Writing – review & editing, Writing – original draft, Validation, Supervision, Resources, Project administration, Methodology, Investigation, Funding acquisition, Conceptualization.

Data availability

Data are available through the NOAA National Centers for Environmental Information via the NCEI Ocean Carbon and Acidification Portal (NCEI Accession Number 0290763): https://www.ncei.noaa.gov/data/oceans/ncei/ocads/metadata/0290763.html.

Declaration of competing interest

The authors declare that they have no known competing financial interests or personal relationships that could have appeared to influence the work reported in this paper.

Acknowledgements

We thank the Editor and the anonymous reviewers for their useful comments. We thank Matan Yona, Adam Levi and Sharon Ram for help during the culture and the analytical work. Thanks also to Shai Oron, Oriya Moav and Tanya Rivlin for the field collections in Eilat, and for the IUI for the use of their boat and dive facilities. This study is funded by NSF-BSF project 1634573 and by ISF project 790/16 and 1886/20. FIERCE is financially supported by the Deutsche Forschungsgemeinschaft (DFG: INST 161/921-1 FUGG, INST 161/923-1 FUGG and INST 161/1073-1 FUGG), and received financial support from the Wilhelm and Else Heraeus Foundation, which is gratefully acknowledged. This is FIERCE contribution No. 179.

Appendix A. Supplementary material

There are two supporting information files: (1) text with additional LA-ICPMS methodological details and foraminifera growth rate discussion, and (2) Figures S1–S5 and Tables S1–S7. Supplementary material to this article can be found online at https://doi.org/10.1016/j.gca.2024.11.022.

References

Addadi, L., Raz, S., Weiner, S., 2003. Taking advantage of disorder: amorphous calcium carbonate and its roles in biomineralization. Adv. Mater. 15 (12), 959–970.
Aizenberg, J., Addadi, L., Weiner, S., Lambert, G., 1996. Stabilization of amorphous calcium carbonate by specialized macromolecules in biological and synthetic precipitates. Adv. Mater. 8 (3), 222–226.
Allen, K.A., Hönisch, B., Eggins, S.M., Haynes, L.L., Rosenthal, Y., Yu, J., 2016. Trace element proxies for surface ocean conditions: A synthesis of culture calibrations with planktic foraminifera. Geochim. Cosmochim. Acta 193, 197–221.
Arns, A.I., Evans, D., Schiebel, R., Fink, L., Mezger, M., Alig, E., Linckens, J., Jochum, K. P., Schmidt, M.U., Jantschke, A., Haug, G.H., 2022. Mesocrystalline architecture in hyaline foraminifer shells indicates a non-classical crystallisation pathway. Geochemistry, Geophys. Geosystems, 1–18.
Beniash, E., Aizenberg, J., Addadi, L., Weiner, S., 1997. Amorphous calcium carbonate transforms into calcite during sea urchin larval spicule growth. Proc. R. Soc. Lond. B 264 (1380), 461–465.
Bentov, S., Brownlee, C., Erez, J., 2009. The role of seawater endocytosis in the biomineralization process in calcareous foraminifera. Proc. Natl. Acad. Sci. u. s. a. 106, 21500–21504.
Bentov, S., Erez, J., 2005. Novel observations on biomineralization processes in foraminifera and implications for Mg/Ca ratio in the shells. Geology 33 (11), 841–844.
Bentov, S., Erez, J., 2006. Impact of biomineralization processes on the Mg content of foraminiferal shells: A biological perspective. Geochemistry, Geophys. Geosystems 7 (1).
Berner, R.A., Lasaga, A.C., Garrels, R.M., 1983. Carbonate-silicate geochemical cycle and its effect on atmospheric carbon dioxide over the past 100 million years. Am. J. Sci., 283 (7).
Blue, C.R., Giuffre, A., Mergelsberg, S., Han, N., De Yoreo, J.J., Dove, P.M., 2017. Chemical and physical controls on the transformation of amorphous calcium carbonate into crystalline $CaCO_3$ polymorphs. Geochim. Cosmochim. Acta 196, 179–196.
Brasier, M.D., Green, O.R., 1993. Winners and losers: stable isotopes and microhabitats of living Archaiadae and Eocene Nummulites (larger foraminifera). Mar. Micropaleontol. 20 (3–4), 267–276.
Busenberg, E., Plummer, L.N., 1985. Kinetic and thermodynamic factors controlling the distribution of SO_4^{2-} and Na^+ in calcites and selcted aragonites. Geochim. Cosmochim. Acta 49, 713–725.
Coenen, D., Evans, D., Hauzer, H., Nambiar, R., Jurikova, H., Dumont, M., Müller, W., 2024. Boron isotope pH calibration of a shallow dwelling benthic nummulitid foraminifera. Geochim. Cosmochim. Acta 378, 217–233.
De Choudens-Sanchez, V., Gonzalez, L.A., 2009. Calcite and Aragonite Precipitation Under Controlled Instantaneous Supersaturation: Elucidating the Role of $CaCO_3$ Saturation State and Mg/Ca Ratio on Calcium Carbonate Polymorphism. J. Sediment. Res. 79, 363–376.
De Nooijer, L.D., Spero, H.J., Erez, J., Bijma, J., Reichart, G.J., 2014. Biomineralization in perforate foraminifera. Earth Sci. Rev. 135, 48–58.
de Nooijer, L.J., Toyofuku, T., Kitazato, H., 2009. Foraminifera promote calcification by elevating their intracellular pH. Proc. Natl. Acad. Sci. 106 (36), 15374–15378.
Devriendt, L.S., Mezger, E.M., Olsen, E.K., Watkins, J.M., Kaczmarek, K., Nehrke, G., de Nooijer, L.J., Reichart, G.J., 2021. Sodium incorporation into inorganic $CaCO_3$ and implications for biogenic carbonates. Geochim. Cosmochim. Acta 314, 294–312.
Dissard, D., Nehrke, G., Reichart, G.J., 2009. Impact of seawater pCO_2 changes on calcification and on Mg/Ca and Sr/Ca in benthic foraminifera calcite (*Ammonia tepida*): results from culturing experiments. Biogeosciences Discuss. 6, 3771–3802.
Dueñas-Bohórquez, A., da Rocha, R.E., Kuroyanagi, A., Bijma, J., Reichart, G.J., 2009. Effect of salinity and seawater calcite saturation state on Mg and Sr incorporation in cultured planktonic foraminifera. Mar. Micropaleontol. 73, 178–189.
Erez, J., 2003. The source of ions for biomineralization in foraminifera and their implications for paleoceanographic proxies (Review). Rev. Mineral. Geochemistry 54, 115.
Evans, D., Erez, J., Oron, S., Müller, W., 2015. Mg/Ca-temperature and seawater-test chemistry relationships in the shallow-dwelling large benthic foraminifera *Operculina ammonoides*. Geochim. Cosmochim. Acta 148, 325–342.
Evans, D., Wade, B.S., Henehan, M., Erez, J., Müller, W., 2016. Revisiting carbonate chemistry controls on planktic foraminifera Mg/Ca: Implications for sea surface temperature and hydrology shifts over the Paleocene-Eocene Thermal Maximum and Eocene-Oligocene transition. Clim. past 12, 819–835.
Evans, D., Müller, W., 2018. Automated extraction of a five-year LA-ICP-MS trace element data set of ten common glass and carbonate reference materials: Long-term data quality, optimisation and laser cell homogeneity. Geostand. Geoanal. Res. 42 (2), 159–188.
Evans, D., Müller, W., Erez, J., 2018. Assessing foraminifera biomineralisation models through trace element data of cultures under variable seawater chemistry. Geochim. Cosmochim. Acta 236, 198–217.
Evans, D., Webb, P.B., Penkman, K., Kroger, R., Allison, N., 2019. The characteristics and biological relevance of inorganic amorphous calcium carbonate (ACC) precipitated from seawater. Cryst. Growth Des. 19 (8), 4300–4313.
Evans, D., Gray, W.R., Rae, J.W.B., Greenop, R., Webb, P.B., Penkman, K., Kröger, R., Allison, N., 2020. Trace and major element incorporation into amorphous calcium carbonate (ACC) precipitated from seawater. Geochim. Cosmochim. Acta 290, 293–311.
Füger, A., Konrad, F., Leis, A., Dietzel, M., Mavromatis, V., 2019. Effect of growth rate and pH on lithium incorporation in calcite. Geochim. Cosmochim. Acta 248, 14–24.
Gabitov, R., Sadekov, A., Yapaskurt, V., Borrelli, C., Bychkov, A., Sabourin, K., Perez-Huerta, A., 2019. Elemental uptake by calcite slowly grown from seawater solution: An In-situ study via depth profiling. Front. Earth Sci. 7, 1–11.
Geerken, E., de Nooijer, L., Toyofuku, T., Roepert, A., Middelburg, J.J., Kienhuis, M.V. M., Nagai, Y., Polerecky, L., Reichart, G.J., 2022. High precipitation rates characterize biomineralization in the benthic foraminifer *Ammonia beccarii*. Geochim. Cosmochim. Acta 318, 70–82.
Gray, W.R., Evans, D., 2019. Nonthermal Influences on Mg/Ca in Planktonic Foraminifera: A Review of Culture Studies and Application to the Last Glacial Maximum supporting information. Paleoceanogr. Paleoclimatology 34, 306–315.
Hauzer, H., Evans, D., Müller, W., Rosenthal, Y., Erez, J., 2018. Calibration of Na partitioning in the calcitic foraminifer *Operculina ammonoides* under variable Ca concentration: Toward reconstructing past seawater composition. Earth Planet. Sci. Lett. 497, 80–91.
Hauzer, H., Evans, D., Müller, W., Rosenthal, Y., Erez, J., 2021. Salinity Effect on Trace Element Incorporation in Cultured Shells of the Large Benthic Foraminifer *Operculina ammonoides*. Paleoceanogr. Paleoclimatology 36, 1–19.
Heinrich, C.A., Pettke, T., Halter, W.E., Aigner-Torres, M., Audétat, A., Günther, D., Hattendorf, B., Bleiner, D., Guillong, M., Horn, I., 2003. Quantitative multi-element analysis of minerals, fluid and melt inclusions by laser-ablation inductively-coupled-plasma mass-spectrometry. Geochim. Cosmochim. Acta 67 (18), 3473–3497.
Henehan, M.J., Rae, J.W.B., Foster, G.L., Erez, J., Prentice, K.C., Kucera, M., Bostock, H. C., Martínez-Botí, M.A., Milton, J.A., Wilson, P.A., Marshall, B.J., Elliott, T., 2013. Calibration of the boron isotope proxy in the planktonic foraminifera Globigerinoides ruber for use in palaeo-CO2 reconstruction. Earth Planet. Sci. Lett. 364, 111–122.
Holland, K., Eggins, S.M., Hönisch, B., Haynes, L.L., Branson, O., 2017. Calcification rate and shell chemistry response of the planktic foraminifer *Orbulina universa* to changes in microenvironment seawater carbonate chemistry. Earth Planet. Sci. Lett. 464, 124–134.

Horita, J., Zimmermann, H., Holland, H.D., 2002. Chemical evolution of seawater during the Phanerozoic: Implications from the record of marine evaporites. Geochim. Cosmochim. Acta 66 (21), 3733–3756.
Jacob, D.E., Wirth, R., Agbaje, O.B.A., Branson, O., Eggins, S.M., 2017. Planktic foraminifera form their shells via metastable carbonate phases. Nat. Commun. 8, 1–9.
Keul, N., Langer, G., Thoms, S., de Nooijer, L.J., Reichart, G.J., Bijma, J., 2017. Exploring foraminiferal Sr/Ca as a new carbonate system proxy. Geochim. Cosmochim. Acta 202, 374–386.
Kısakürek, B., Eisenhauer, A., Böhm, F., Garbe-Schönberg, D., Erez, J., 2008. Controls on shell Mg/Ca and Sr/Ca in cultured planktonic foraminiferan, *Globigerinoides ruber* (white). Earth Planet. Sci. Lett. 273, 260–269.
Kitano, Y., Okumura, M., Idogaki, M., 1975. Incorporation of sodium, chloride and sulfate with calcium carbonate. Geochem. J. 9, 75–84.
Land, L.S., Hoops, G.K., 1973. Sodium in carbonate sediments and rocks: a possible index to the salinity of diagenetic solutions. J. Sediment. Petrol. 43, 614–617.
Lawson, V.J., Rosenthal, Y., Bova, S.C., Lambert, J., Linsley, B.K., Bu, K., et al., 2024. Controls on Sr/Ca, S/Ca, and Mg/ Ca in benthic foraminifera: Implications for the carbonate chemistry of the Pacific Ocean over the last 350 ky. Geochem. Geophys. Geosyst. 25.
Le Houedec, S., Erez, J., Rosenthal, Y., 2021. Testing the influence of changing seawater Ca concentration on Elements/Ca ratios in planktic foraminifera: A culture experiment. Geochem. Geophys. Geosyst. 22 (3).
Lea, D.W., Mashiotta, T., a. and Spero H. J., 1999. Controls on magnesium and strontium uptake in planktonic foraminifera determined by live culturing. Geochim. Cosmochim. Acta 63, 2369–2379.
Lorens, R.B., 1981. Sr, Cd, Mn and Co distribution coefficients in calcite as a function of calcite precipitation rate. Geochim. Cosmochim. Acta 45, 553–561.
Maloy, S.R., (1990). Sodium-coupled cotransport. Krulwich, T. (Ed.) Bacterial energetics: A treatise on structure and function (Vol. 7). 203-224, Elsevier.
Marriott, C.S., Henderson, G.M., Crompton, R., Staubwasser, M., Shaw, S., 2004. Effect of mineralogy, salinity, and temperature on Li/Ca and Li isotope composition of calcium carbonate. Chem. Geol. 212, 5–15.
Martens, L., Stassen, P., Steurbaut, E., Speijer, R.P., 2022. Assessing *Nummulites* geochemistry as a proxy for early Eocene palaeotemperature evolution in the North Sea Basin. J. Geol. Soc. London 179 (4).
Mavromatis, V., Gautier, Q., Bosc, O., Schott, J., 2013. Kinetics of Mg partition and Mg stable isotope fractionation during its incorporation in calcite. Geochim. Cosmochim. Acta 114, 188–203.
Mojtahid, M., Depuydt, P., Mouret, A., Le Houedec, S., Fiorini, S., Chollet, S., Massol, F., Dohou, F., Filipsson, H.L., Boer, W., Reichart, G.J., Barras, C., 2023. Assessing the impact of different carbonate system parameters on benthic foraminifera from controlled growth experiments. Chem. Geol. 623, 121396.
Mucci, A., Morse, J.W., 1983. The incorporation of Mg^{2+} and Sr^{2+} into calcite overgrowths: influences of growth rate and solution composition. Geochim. Cosmochim. Acta 47, 217–233.
Müller, M.N., Blanco-Ameijeiras, S., Stoll, H.M., Mendez-Vicente, A., Lebrato, M., 2021. Temperature Induced Physiological Reaction Norms of the Coccolithophore *Gephyrocapsa oceanica* and Resulting Coccolith Sr/Ca and Mg/Ca Ratios. Front. Earth Sci. 9, 1–9.
Nambiar, R., Hauzer, H., Gray, W.R., Henehan, M.J., Cotton, L., Erez, J., Rosenthal, Y., Renema, W., Müller, W., Evans, D., 2023. Controls on potassium incorporation in foraminifera and other marine calcifying organisms. Geochim. Cosmochim. Acta 351, 125–138.
Nehrke, G., Keul, N., Langer, G., De Nooijer, L.J., Bijma, J., Meibom, A., 2013. A new model for biomineralization and trace-element signatures of Foraminifera tests. Biogeosciences 10, 6759–6767.
Okumura, M., Kitano, Y., 1986. Coprecipitation of alkali metal ions with calcium carbonate. Geochim. Cosmochim. Acta 50, 49–58.
Oron, S., Evans, D., Abramovich, S., Almogi-Labin, A., Erez, J., 2020. Differential sensitivity of a symbiont-bearing foraminifer to seawater carbonate chemistry in a decoupled DIC-pH experiment. J. Geophys. Res. Biogeosciences 1–16.
Poet, M., Vigier, N., Bouret, Y., Jarretou, G., Gautier, R., Bendahhou, S., Balter, V., Montanes, M., Thibon, F., Counillon, L., 2023. Biological fractionation of lithium isotopes by cellular Na^+/H^+ exchangers unravels fundamental transport mechanisms. Iscience 26 (6).
Rae, J.W.B., Zhang, Y.G., Liu, X., Foster, G.L., Stoll, H.M., Whiteford, R.D.M., 2021. Atmospheric CO_2 over the past 66 million years from marine archives. Annu. Rev. Earth Planet. Sci. 49, 609–641.
Ram, S., Erez, J., 2021. The Distribution Coefficients of Major and Minor Elements in Coral Skeletons Under Variable Calcium Seawater Concentrations. Front. Earth Sci. 9, 1–14.
Ram, S., Erez, J., 2023. Anion elements incorporation into corals skeletons: Experimental approach for biomineralization and paleo-proxies. Proc. Natl. Acad. Sci. 120 (45).
Rickaby, R.E.M., Schrag, D.P., Zondervan, I., Riebesell, U., 2002. Growth rate dependence of Sr incorporation during calcification of *Emiliania huxleyi*. Global Biogeochem. Cycles 16 (1), 6.
Roberts, J., Kaczmarek, K., Langer, G., Skinner, L.C., Bijma, J., Bradbury, H., Turchyn, A. V., Lamy, F., Misra, S., 2018. Lithium isotopic composition of benthic foraminifera: A new proxy for paleo-pH reconstruction. Geochim. Cosmochim. Acta 236, 336–350.
Russell, A.D., Hönisch, B., Spero, H.J., Lea, D.W., 2004. Effects of seawater carbonate ion concentration and temperature on shell U, Mg, and Sr in cultured planktonic foraminifera. Geochim. Cosmochim. Acta 68, 4347–4361.
Seyedali, M., Coogan, L.A., Gillis, K.M., 2021. The effect of solution chemistry on elemental and isotopic fractionation of lithium during inorganic precipitation of calcite. Geochim. Cosmochim. Acta 311, 102–118.
Stoll, H.M., Schrag, D.P., 2000. Coccolith Sr/Ca as a new indicator of coccolithophorid calcification and growth rate. Geochem. Geophys. Geosyst. 1 (5).
Taylor, A.R., Brownlee, C., Wheeler, G.L., 2012. Proton channels in algae: reasons to be excited. Trends Plant Sci. 17 (11), 675–684.
Ulrich, R.N., Guillermic, M., Campbell, J., Hakim, A., Han, R., Singh, S., Stewart, J.D., Román-Palacios, C., Carroll, H.M., De Corte, I., Gilmore, R.E., Doss, W., Tripati, A., Ries, J.B., Eagle, R.A., 2021. Patterns of element incorporation in calcium carbonate biominerals recapitulate phylogeny for a diverse range of marine calcifiers. Front. Earth Sci. 9.
van Dijk, I., de Nooijer, L.J., Wolthers, M., Reichart, G.J., 2017. Impacts of pH and $[CO_3^{2-}]$ on the incorporation of Zn in foraminiferal calcite. Geochim. Cosmochim. Acta 197, 263–277.
Vigier, N., Rollion-Bard, C., Levenson, Y., Erez, J., 2015. Lithium isotopes in foraminifera shells as a novel proxy for the ocean dissolved inorganic carbon (DIC). Comptes Rendus - Geosci. 347, 43–51.
Westerhold, T., Marwan, N., Drury, A.J., Liebrand, D., Agnini, C., Anagnostou, E., Barnet, J.S.K., Bohaty, S.M., Vleeschouwer, D., De, F.F., Frederichs, T., Hodell, D.A., Holbourn, A.E., Kroon, D., Lauretano, V., Littler, K., Lourens, L.J., Lyle, M., Palike, H., Rohl, U., Tian, J., Wilkens, R.H., Wilson, P.A., Zachos, J.C., 2020. An astronomically dated record of Earth's climate and its predictability over the last 66 million years. Science 369 (6509), 1383–1387.
White, A.F., 1977. Sodium and potassium coprecipitation in aragonite. Geochim. Cosmochim. Acta 41, 613–625.
White, A.F., 1978. Sodium coprecipitation in calcite and dolomite. Chem. Geol. 23, 65–72.
Yoshimura, T., Tamenori, Y., Suzuki, A., Kawahata, H., Iwasaki, N., Hasegawa, H., Nguyen, L.T., Kuroyanagi, A., Yamazaki, T., Kuroda, J., Ohkouchi, N., 2017. Altervalent substitution of sodium for calcium in biogenic calcite and aragonite. Geochim. Cosmochim. Acta 202, 21–38.
Yu, J., Elderfield, H., 2007. Benthic foraminiferal B/Ca ratios reflect deep water carbonate saturation state. Earth Planet. Sci. Lett. 258, 73–86.
Yu, J., Elderfield, H., Jin, Z., Tomascak, P., Rohling, E.J., 2014. Controls on Sr/Ca in benthic foraminifera and implications for seawater Sr/Ca during the late Pleistocene. Quat. Sci. Rev. 98, 1–6.
Zachos, J., Pagani, M., Sloan, L., Thomas, E., & Billups, K. (2001). Trends, rhythms, and aberrations in global climate 65 Ma to present. science, 292(5517), 686-693.Zeebe, R. E., and Sanyal, A. (2002). Comparison of two potential strategies of planktonic foraminifera for house building: Mg^{2+} or H^+ removal?. Geochimica et Cosmochimica Acta, 66(7), 1159-1169.
Zeebe, R.E., Sanyal, A., 2002. Comparison of two potential strategies of planktonic foraminifera for house building: Mg2+ or H+ removal? Geochim. Cosmochim. Acta 66 (7), 1159–1169.
Zeebe, R.E., Tyrrell, T., 2019. History of carbonate ion concentration over the last 100 million years II: Revised calculations and new data. Geochim. Cosmochim. Acta 257, 373–392.
Zeebe, R.E., Wolf-Gladrow, D., 2001. CO2 in Seawater: Equilibrium, Kinetics, Isotopes, No. 65. Gulf Professional Publishing.
Zhou, X., Rosenthal, Y., Haynes, L., Si, W., Evans, D., Huang, K.F., Hönisch, B., Erez, J., 2021. Planktic foraminiferal Na/Ca: A potential proxy for seawater calcium concentration. Geochim. Cosmochim. Acta 305, 306–322.
Zhu, C., Chen, T., Zhao, L., 2021. Magnesium partitioning into vaterite and its potential role as a precursor phase in foraminiferal Mg/Ca thermometer. Earth Planet. Sci. Lett. 567, 116989.